

Modification of vortex liquid structure and dynamics of a $\text{Bi}_2\text{Sr}_2\text{CaCu}_2\text{O}_{8+\delta}$ single crystal induced by excessive-oxygen doping

D. Darminto

Department of Physics, Faculty of Mathematics and Science, Sepuluh Nopember Institute of Technology, Sukolilo, Surabaya 60111, Indonesia

A. A. Menovsky

Van der Waals-Zeeman Institute, University of Amsterdam, Valckenierstraat 65, 1018 XE Amsterdam, The Netherlands

M. O. Tjia

Department of Physics, Bandung Institute of Technology, Jl. Ganesa 10, Bandung 40132, Indonesia
(Received 3 September 2002; published 30 January 2003)

A study has been carried out on the vortex liquid state of $\text{Bi}_2\text{Sr}_2\text{CaCu}_2\text{O}_{8+\delta}$ single crystal with excessive-oxygen doping based on its magnetotransport data. The enhanced disorder and reduced anisotropy due to excessive oxygen content are shown to give rise to the $U \sim H^{-1}$ behavior for the activation energy of thermally assisted flux flow (TAFF), observed in the Bi-based system. This study has also revealed the existence of high and low-TAFF regimes supporting a previous report on the existence of a theoretically predicted disentangled vortex line liquid phase.

DOI: 10.1103/PhysRevB.67.012503

PACS number(s): 74.25.Dw, 74.25.Fy, 74.72.Hs

One of the intensively studied features of the vortex matter in cuprate superconductors is the vortex dynamics associated with the pinning mechanism of the vortex lines in the liquid state. This pinning mechanism is known to depend generally on the pinning energy at the pinning centers created by structural disorder, and the elastic or plastic energy of the vortex line system related to its degree of anisotropy. These effects are embodied in the activation energy $U(H, T)$ for the hopping motion of the fluxoids, and should thus characterize the magnetoresistive behavior $\rho(T, H)$ of the superconductor. Theoretical models for vortex liquid have predicted $U \sim H^{-\alpha}$ behavior with $\alpha = 1$ for elastic shear^{1,2} and $\alpha = 0.5$ for plastic flow³ in three-dimensional (3D) vortex matter, whereas a 2D system is expected to exhibit a distinct $U \sim \ln H$ variation.^{4,5} Convincing experimental verification has so far been obtained mainly for samples of low anisotropy such as $\text{YBa}_2\text{Cu}_3\text{O}_{7-\delta}$ (Y-123).^{6,7} In the case of $\text{Bi}_2\text{Sr}_2\text{CaCu}_2\text{O}_{8+\delta}$ (Bi-2212) samples, we are still confronted with a rather wide-ranging variation of α and even discrepancies between results of fitting experimental data of $U(H)$ in both the 3D and 2D regimes.⁸⁻¹⁴ Additionally, the correlation between high-low thermally assisted flux flow (TAFF) regimes reported before^{5,15} and the predicted entangled-disentangled vortex liquid phases have not been seriously addressed.

In this experiment, a series of magnetotransport measurements were performed on a Bi-2212 crystal, excessively doped with oxygen. The enhancement of disorder and reduction of anisotropy thus induced were studied by their effects on the characteristic transition of magnetoresistivity curves and its corresponding melting behavior of the sample. The field-dependent behavior of the activation energy U was thereby deduced by a well-known standard procedure. Additionally, possible correlation of the high- and low-TAFF regimes with different vortex line topologies was examined and discussed in relation with enhanced disorder and reduced anisotropy effects. The results of these analyses were sum-

marized in a vortex phase diagram of the liquid state, where the resulted phase boundaries were fitted with existing theoretical models.

The high quality Bi-2212 single crystal with excessive-oxygen content has been produced by introducing the oxygen into the material in two steps. First, the growing process employing the traveling solvent floating-zone method in a four-mirror furnace of Crystal System Inc. was conducted in a pure oxygen environment with a total pressure of 2.5 atm. This process was designed to yield the oxygen-overdoped sample. The detailed description of this part of the process was already reported elsewhere.¹⁶ Next, the as-grown crystal was cleaved and then post annealed in pure oxygen atmosphere with a total pressure of 2.1 atm at 400°C for 60 h to produce the sample with $T_{c,on} \sim 70$ K. In connection with its relatively low $T_{c,on}$ compared to samples overdoped with oxygen, this sample is considered to be highly overdoped (HO) with oxygen. The $\rho_{ab}(T, H)$ curves were measured using the standard dc four-probe method in the temperature range of 20–250 K with the magnetic field applied parallel to the c -axis, and varied stepwise from 100 Oe to 40 kOe.¹⁶ For the purpose of more comprehensive correlational study of oxygen doping effects, our previous result from optimally doped (OP) sample¹⁷ will also be included in the discussion within the current context.

Depicted in Figs. 1(a) and 1(b) are the $\rho_{ab}(T)$ curves of the OP and HO samples, respectively, in the low magnetic fields up to 1 kOe. The first feature to be noted from the curves is the clear sign of first-order melting transition at $H = 100$ Oe and 200 Oe exhibited by the OP sample as indicated by the arrow heads. Meanwhile, no sign of such a sharp drop of $\rho_{ab}(T)$ is found in the HO sample in the entire range of magnetic field applied in this experiment (the higher-field data are not shown here). Instead, a change of slope signifying a more gradual transition leads to a “shoulder” structure marked by the dotted line in Fig. 1(b). This is supposed to be indicative of the disorder effect introduced by

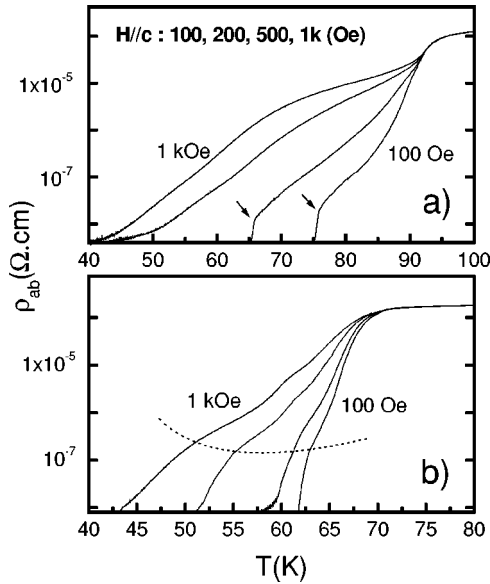


FIG. 1. In-plane resistive transition curves measured on the (a) OP and (b) HO samples in low magnetic fields applied parallel along the c axis. Arrow heads in (a) indicate sharp melting transition and the dotted line in (b) marks the “shoulder” structures as explained in the text.

excessive-oxygen doping. A second feature to be pointed out is the significant reduction of magnetic-induced transitional broadening (ΔT) due to the enhanced pinning effect in the dissipative region. Applying the formula² $\Delta T \sim H^\beta$ to the data, we obtained a good fit with $\beta = 1.16$ and 0.52 for the OP and HO samples, respectively. These results should be viewed as an evidence of enhanced pinning effect in the resistive regime arising from an enlarged number of pinning centers created by increased disorder, combined with strengthened interlayer coupling associated with reduced anisotropy.

In order to proceed further with the dynamical aspects of vortex matter in the dissipative region, we shall invoke the TAFF model which is generally expressed in the well-known Arrhenius form:¹⁸ $\rho(T, H) = \rho_o \exp[-U(T, H)/k_B T]$. The activation energy $U(T, H)$ is given by one of its most commonly adopted expression⁸ $U(T, H) = U_H [1 - (T/T_c)]$, where U_H is the magnetic-field-dependent activation energy. This specific model further yields the more explicit form for the TAFF resistivity: $\rho(T, H) = \rho_o \exp[-U_H(1/T - 1/T_c)]$. The Boltzmann constant (k_B) in this expression is already included in U_H , and $U(T, H)$ is consequently expressed in terms of kelvin. The $\ln \rho$ vs $1/T$ plots of the OP and HO samples at $H = 200$ Oe are presented in Fig. 2. It is clearly seen from Fig. 2(a) that the thermal activation mechanism governs the flux motion in the range between the melting transition temperature (T_m) and a temperature near T_c , where the curve begins to deviate from the linear behavior. This result demonstrates that vortex dynamics in the resistive region of the OP sample is dominated by the TAFF phenomenon, confirming some previous reports on the same samples.^{8,11,14} In the vicinity of T_c , the flux motion no longer obeys the thermally assisted hopping behavior as it is entering a free (unpinned) flow regime. The flux flow (FF)

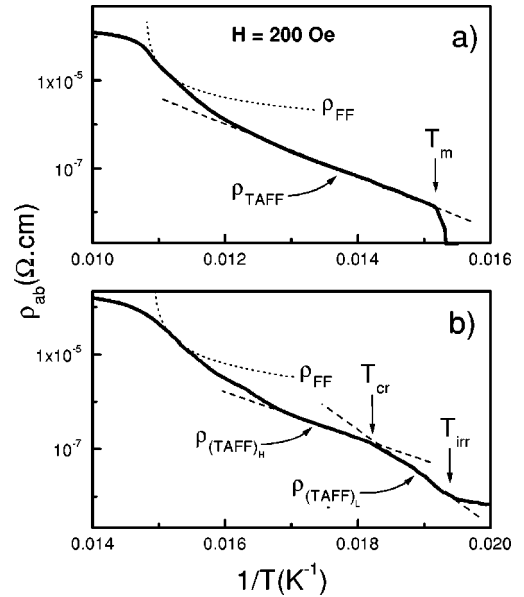


FIG. 2. The ρ_{ab} (in logarithmic scale)— $1/T$ curves in $H = 200$ Oe of the (a) OP and (b) HO samples. The dashed and dotted lines are the best fits of the TAFF and FF models, respectively. The points indicated by T_m , T_{cr} , and T_{irr} are described in the text.

resistivity (ρ_{FF}) in this region is determined according to the classical Bardeen-Stephen model,¹⁹ $\rho_{FF} = \rho_N H/H_{c2}$, where ρ_N is the normal-state resistivity taken at T slightly above $T_{c,on}$ and H_{c2} the upper critical field. The result is plotted in Fig. 2(a) as dotted line, indicating the onsets of the FF regime.

Looking further at the $\ln \rho_{ab} - 1/T$ curve of the HO sample shown in Fig. 2(b), two distinct TAFF regimes manifest themselves on the curve which are obviously separated at T_{cr} (~ 55 K), namely, the crossing temperature where the change of slope occurs on the curve. The TAFF regime of lower resistivity corresponding to higher slope or lower-temperature regime is denoted by (TAFF)_L. This regime spans the temperature range from T_{cr} to the irreversible temperature T_{irr} , obtained from resistivity data by applying the commonly adopted criterion^{12,20} of $\rho_{ab}(T_{irr}) = 10^{-4} \rho_N$. The TAFF regime of higher resistivities, denoted by (TAFF)_H, appears to exist between T_{cr} and the temperature approaching T_c , where the FF regime begins to set in. The existence of these two TAFF regimes has previously been reported on Y-123 (Ref. 5), Y-124 (Ref. 15) samples, an artificial layered MoGe/Ge system,²¹ and our oxygen-overdoped (Bi,Pb)-2212 crystal.²² It is interesting in this connection to recall further our earlier work concerning the dynamical state associated with the disentangled vortex liquid.^{16,22} We have noted in that work that the highest-temperature end of the (TAFF)_L regime at T_{cr} nearly coincided with the temperature T_E of our c -axis resistivity data, $\rho_c(T)$, for which $\rho_c(T_E) = 0$, and hence marking the disappearance of dissipation for longitudinal current flow. It was then suggested that the coincidence of T_{cr} and T_E may be viewed as a sign of crossover from the entangled vortex liquid at $T > T_{cr}$ to the disentangled vortex liquid at $T < T_{cr}$, which was predicted theoretically on the basis of 2D boson model.²³

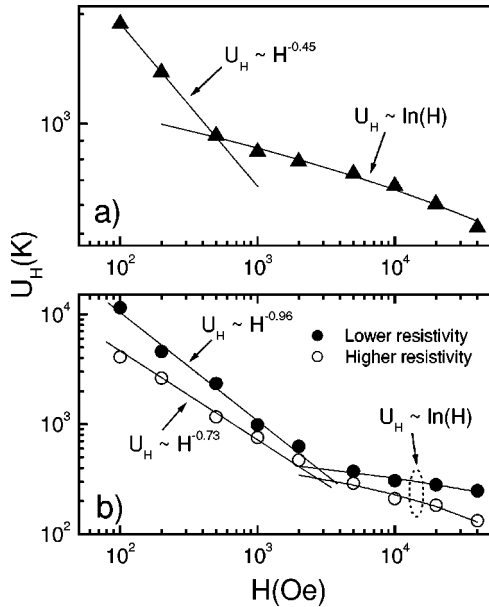


FIG. 3. The TAFF activation energy as function of magnetic field (U_H) of the (a) OP and (b) HO samples. The best fits of the theoretical curves are represented by the solid lines.

For further analysis, we present in Fig. 3 in logarithmic scales the field-dependent activation energy U_H deduced from the $\ln \rho_{ab}-1/T$ curves measured in the range of magnetic field considered in this study. The U_H vs H curve of the OP sample in Fig. 3(a) shows an upward curvature with a clear break at $H \sim 500$ Oe. This breakpoint can be interpreted as a dimensional crossover field of the vortex line solid, H_{2D} .¹² The best fits with the data points, marked by the solid lines in Fig. 3(a), yield the relationships of $U_H = 14\,133/H^{0.45}$ and $U_H = 1432 - 84 \ln(H)$, respectively, for $H < H_{2D}$ and $H > H_{2D}$, delineating a dimensional boundary in good agreement with theoretical predictions.^{4,5} This result is in dire contrast to the data reported by Miu *et al.*¹² on the Bi-2212 thin film, showing a power-law $U(H)$ curve with a fitted value of $\alpha = 0.5$ in $U \sim H^{-\alpha}$ for $H > H_{2D}$. Meanwhile, Fig. 3(b) displays similar qualitative behaviors in both resistive regions for the HO sample, sharing the same features exhibited by the OP sample regarding the functional relationships of $U_H - H$, and the appearance of a breakpoint around H_{2D} . It is found from the best fits on these data, the relations $U_H = 874\,800/H^{0.96}$ and $U_H = 859 - 58 \ln(H)$ for (TAFF)_L regime, corresponding to $H < H_{2D}$ and $H > H_{2D}$, respectively. Similarly, $U_H = 119\,991/H^{0.73}$ and $U_H = 898 - 72 \ln(H)$ for (TAFF)_H regime. Obviously, the activation energy U_H depends less sensitively on H in the HO sample, which is consistent with the lowering of anisotropy and hence an increase of H_{2D} as a result of excessive-oxygen doping and hence the expected decrease in anisotropy. The significance of these observations will be further elaborated below.

It is well known that the collective pinning model^{1,2} predicts the characteristic relation $U \sim 1/H$ for $H_{c1} \ll H \ll H_{c2}$ in the TAFF regime characterized by elastic shear. This $1/H$ dependence is typical to the less anisotropic systems such as Y-123 films and crystals with the reported values of $\alpha = 0.84 - 1.0$.^{6,7,24} Looking back at the result obtained for the

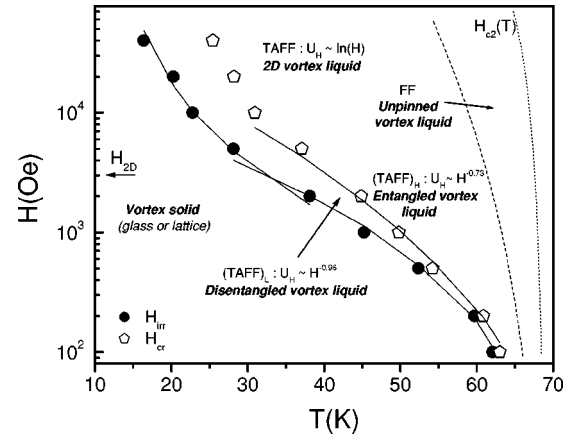


FIG. 4. Vortex phase diagram of the HO sample constructed from magnetotransport data. The solid lines are results of the best fits with theoretical models discussed in the text. The onset of FF regime and upper critical field (H_{c2}) estimated from the data are shown, respectively, by the dashed and dotted lines.

HO sample at $H < H_{2D}$, one notices that $\alpha \approx 1$ in the (TAFF)_L regime. Again, the considerably reduced anisotropy, together with the enhanced disorder of the HO crystal is likely to be responsible for this observation. To the best of our knowledge, no report on the Bi-based superconductors has so far been addressed to this doping induced $(1/H)$ -dependent behavior. As regards to the (TAFF)_H regime, it is useful to recall the plastic flow model proposed by Geshkenbein *et al.*³ The predicted expression of $U_{pl} \sim 1/H^{0.5}$ has generally been verified in more anisotropic materials such as polycrystalline Tl-based film²⁵ and a quasi-two-dimensional multilayer sample of MoGe/Ge.²¹ A relatively broader range of α between 0.16 and 0.70 was found among the anisotropic Bi-2212 polycrystals,⁹ thin-films,^{12,26} as well as single crystals.^{8,11,13,14,27} Our result of $\alpha = 0.45$ obtained from the OP sample is certainly well within the ballpark of the theoretically predicted value. However, the value $\alpha = 0.73$ of the HO sample in the (TAFF)_H regime is somewhat higher than that expected for pure plastic flow. This deviation may be attributed to the elastic contribution arising from the reduced anisotropy caused by the excessive-oxygen doping. In spite of the quantitative difference in α , both the TAFF regime of the OP crystal and the (TAFF)_H regime of the HO crystal are likely to be associated with the entangled vortex liquid phase as implied in our previous studies.^{13,16,22} As the field increases beyond the 3D-2D crossover line, the vortices gradually lose their coherence along the field direction and thereby entering a quasi-2D liquid phase characterized by $U \sim \ln(H)$ dependence of the activation energy. As shown in Fig. 3(b), for both the high- and low-TAFF regimes, a clear break occurs between two distinct curves representing the H -dependent behaviors of the activation energy in the 3D and 2D regions. Even more interesting, the breakpoints for the two cases virtually coincide at a field ~ 3000 Oe, which is none other than the H_{2D} value of the sample.

Plotted further in Fig. 4 is the border between the solid and liquid phases which is represented by the irreversibility

line (IL), $H_{irr}(T)$, determined from the values of T_{irr} for each H in Fig. 2(b). The IL in this case replaces the melting line, $H_m(T)$, which is nonexistent in the HO sample. It is found that two different expressions are needed to fit the $H_{irr}(T)$ data, each of them is only valid for either $H < H_{2D}$ or $H > H_{2D}$ as indicated in Fig. 4 by the solid lines. It was reported in our previous work¹⁶ that the best fits of these data were achieved by the expressions $H_{irr}(T) = 10\,880(1 - T/T_c)^2$ Oe and $H_{irr}(T) = 186 \exp(91.3/T)$ Oe, respectively, for $H < H_{2D}$ and $H > H_{2D}$. The former expression is based on the 3D melting transition model,^{28,29} whereas the latter is deduced from the model of Josephson-coupled layered superconductor describing a quasi-2D vortex melting.³⁰ The melting process in the 3D vortex structure is dominated by the thermal fluctuation effect^{29,31} as indicated by $n=2$ in the $(1 - T/T_c)^n$ dependence of H_{irr} . In the liquid state, one comes across successively the disentangled and entangled vortex liquid phases which are separated by the curve $H_{cr}(T) = 2.9 \times 10^5(1/T - 1/T_c)$ Oe resulted from the best fit of those data for $H < H_{2D}$. The vortex decoupling occurs slightly above H_{2D} and both disentangled and entangled liquid phases transform into the quasi-2D vortex liquid at a higher magnetic field. At higher temperature below the $H_{c2}(T)$ line, the pinned vortex line liquid becomes unpinned and enters the FF regime.

Compared with the vortex phase diagram for our OP sample, which is practically the same as those reported by other researchers and not shown here, one readily observes the large differences affected by excessive-oxygen doping. These are accompanied by roughly one order of magnitude difference in the value of H_{2D} , associated with correspondingly large change in the degree of anisotropy (γ^2). Another major feature arising from the excessive-oxygen doping is the appearance of disentangled vortex liquid phase separat-

ing the entangled liquid phase from the solid vortex phase, and bounded from above by H_{2D} . Although its existence was predicted theoretically²³ and indicated previously in a Pb-substituted Bi-2212 overdoped with oxygen,²² the experimental evidence for this liquid phase has so far evaded experimental observation in the Bi-based system with lower-oxygen-doping levels.

In conclusion, we have presented in this report interesting effects induced by excessive-oxygen doping in Bi-2212 single crystal. The existence of two different liquid phases associated with the low- and high-TAFF regimes, and their respective correlations with the entangled and disentangled vortex line liquid phases are clearly demonstrated, confirming a previous observation of longitudinal coherency in the disentangled phase. The excessive-oxygen doping has also been shown to yield the first evidence of $U \sim H^{-\alpha}$ with $\alpha \approx 1$ in the Bi-based system. These results which are summarized by the vortex liquid phase diagram clearly reveal the roles of strong disorder and reduced anisotropy induced by excessive-oxygen doping of the crystal.

We gratefully acknowledge FOM-ALMOS and K. Kishio for the use of crystal growth apparatus and measurement facilities, respectively. We would also like to thank J. Shimoyama for fruitful discussions, T. Motohashi, Y. Nakayama, H. Kobayashi, T. Yamada, A.A. Nugroho, and I.M. Sutjahja for their valuable technical assistance. This work was also partially supported by RUT research grant, under the Contract No. 207/SP/RUT/BPPT/IV/97 of Indonesia, and by KNAW under the Project No. 95-BTM-33 of The Netherlands. One of us (D.D.) would like to thank FOM-ALMOS and The Matsumae International Foundation for supporting his research activities at The University of Amsterdam and The University of Tokyo, respectively.

- ¹Y. Yeshurun and A.P. Malozemoff, Phys. Rev. Lett. **60**, 2202 (1988).
²M. Thinkam, Phys. Rev. Lett. **61**, 1658 (1988).
³V.B. Geshkenbein *et al.*, Physica C **162-164**, 239 (1989).
⁴S.P. Obukov and M. Rubenstein, Phys. Rev. Lett. **65**, 1279 (1990).
⁵X.G. Qiu *et al.*, Phys. Rev. B **52**, 559 (1995).
⁶J.Z. Sun *et al.*, Appl. Phys. Lett. **54**, 663 (1989); T.T.M. Palstra, *et al.*, *ibid.* **54**, 763 (1989).
⁷Y. Eltsev, W. Holm, and O. Rapp, Phys. Rev. B **49**, 12333 (1994).
⁸T.T.M. Palstra *et al.*, Phys. Rev. Lett. **61**, 1662 (1988).
⁹P. Mandel *et al.*, Physica C **169**, 43 (1990).
¹⁰T. Fukami *et al.*, Physica C **159**, 422 (1989).
¹¹T.W. Krausse *et al.*, Physica C **224**, 13 (1994).
¹²L. Miu *et al.*, Phys. Rev. B **57**, 3151 (1998).
¹³D. Darminto *et al.*, in *Proceeding of the Second Magneto-Electronic International Symposium*, edited by A. Matsumoto and K. Ito (Shinshu University, Nagano, 1999), p. 243.
¹⁴W. Chen, J.P. Franck, and J. Jung, Physica C **341-348**, 1195 (2000).
¹⁵X.G. Qiu *et al.*, Phys. Rev. B **58**, 8826 (1998).
¹⁶D. Darminto, M.O. Tjia, and A.A. Menovsky, Physica C **341-348**,

- 1323 (2000).
¹⁷D. Darminto *et al.*, Physica C **357-360**, 617 (2001).
¹⁸P.H. Kes *et al.*, Supercond. Sci. Technol. **1**, 242 (1989).
¹⁹J. Bardeen and M.J. Stephen, Phys. Rev. **140**, A1197 (1965).
²⁰D.T. Fuchs *et al.*, Phys. Rev. B **54**, R796 (1996).
²¹D.G. Steel, W.R. White, and J.M. Greybeal, Phys. Rev. Lett. **71**, 161 (1993).
²²D. Darminto *et al.*, Phys. Rev. B **62**, 6649 (2000).
²³D. R. Nelson, in *Phenomenology and Applications of High Temperature Superconductors*, edited by K. Bedell *et al.* (Addison-Wesley, New York, 1991).
²⁴M. Anderson, A. Rydh, and O. Rapp, Physica C **341-348**, 1239 (2000).
²⁵K.C. Woo *et al.*, Phys. Rev. Lett. **63**, 1877 (1989).
²⁶J.T. Kucera *et al.*, Phys. Rev. B **46**, 11 004 (1992).
²⁷D. Shi *et al.*, Phys. Rev. B **43**, 514 (1991).
²⁸A. Houghton, R. Pelcovits, and A. Sudbo, Phys. Rev. B **40**, 6763 (1989).
²⁹C.C. Almasan *et al.*, Phys. Rev. Lett. **69**, 3812 (1992).
³⁰F. Zuo *et al.*, Phys. Rev. B **52**, R755 (1995).
³¹G. Blatter and B. Ivlev, Phys. Rev. Lett. **70**, 2621 (1993).